Journal of Power Sources 218 (2012) 348–351

Contents lists available at SciVerse ScienceDirect

Journal of Power Sources

journal homepage: www.elsevier.com/locate/jpowsour

Short communication

3D Non-destructive morphological analysis of a solid oxide fuel cell anode using full-field X-ray nano-tomography

Yu-chen Karen Chen-Wiegart [a], J. Scott Cronin [b], Qingxi Yuan [a], Kyle J. Yakal-Kremski [b], Scott A. Barnett [b], Jun Wang [a,*]

[a] Photon Science Directorate, Brookhaven National Laboratory, 75 Brookhaven Avenue, Bldg. 725D, Upton, NY 11973, USA
[b] Department of Materials Science and Engineering, Northwestern University, 2220 Campus Drive, Evanston, IL 60208, USA

HIGHLIGHTS

- Best 3D resolution and unique large analyzed volume for the first time.
- 3D morphological analysis with unprecedented statistical accuracy.
- The anode resistance predicted from 3D data in good agreement with experiment.
- Newly developed unique automated full field X-ray nano-tomography

ARTICLE INFO

Article history:
Received 18 April 2012
Received in revised form
26 June 2012
Accepted 28 June 2012
Available online 16 July 2012

Keywords:
Solid oxide fuel cell
Transmission X-ray microscopy
3D analysis
Nano-tomography and computed tomography
Electrochemical impedance spectroscopy

ABSTRACT

An accurate 3D morphological analysis is critically needed to study the process–structure-property relationship in many application fields such as battery electrodes, fuel cells and porous materials for sensing and actuating. Here we present the application of a newly developed full field X-ray nano-scale transmission microscopy (TXM) imaging for a non-destructive, comprehensive 3D morphology analysis of a porous Ni–YSZ solid oxide fuel cell anode. A unique combination of improved 3D resolution and large analyzed volume (~3600 μm^3) yields structural data with excellent statistical accuracy. 3D morphological parameters quantified include phase volume fractions, surface and interfacial area densities, phase size distribution, directional connectivity, tortuosity, and electrochemically active triple phase boundary density. A prediction of electrochemical anode polarization resistance based on this microstructural data yielded good agreement with a measured anode resistance via electrochemical impedance spectroscopy. The Mclachlan model is used to estimate the anode electrical conductivity.

1. Introduction

Solid oxide fuel cells (SOFCs) are expected to play a critical role in future electricity generation by providing increased energy efficiency and reduced pollution [1]. SOFC nickel–yttria stabilized zirconia (Ni–YSZ) anodes provide an excellent example of the advantages of the emerging TXM method because electrochemical performance is strongly related to 3D microstructure. Furthermore, the TXM results can be compared with 3D reconstruction data of Ni–YSZ SOFC anodes obtained using other methods, either serial sectioning by focused-ion-beam-scanning electron-microscopy (FIB-SEM) [1–6] or nano-tomography by full field transmission X-ray microscopy (TXM) using hard X-ray (5–11 keV) [2,7–9]. While most of the prior work and the best quality data has so far been obtained using FIB-SEM [1–6], the emerging full-field nano-scale TXM X-ray imaging technique brings a few significant advantages: 1) non-destructive measurement without sectioning sample and filling pores with epoxy, allowing continuous morphological evolution studies from the same sample, 2) elemental and chemical sensitivity achieved by imaging near the X-ray absorption edge of an element, 3) potential for doing *in situ* experiments, *e.g.* imaging and electrochemical measurement carried out simultaneously at elevated temperature in a gas/liquid environment, and 4) capability to observe the microstructure of the full cell, including anode, electrolyte, and cathode, in a single measurement. The 3D spatial resolution obtained by TXM is currently below 50 nm [10], comparable to FIB-SEM.

Here we present a comprehensive 3D morphological analysis of a SOFC Ni–YSZ anode using a high-resolution full field X-ray

* Corresponding author. Tel.: +1 631 344 2661; fax: +1 631 344 3238.
E-mail address: junwang@bnl.gov (J. Wang).

0378-7753/$ – see front matter © 2012 Elsevier B.V. All rights reserved.
http://dx.doi.org/10.1016/j.jpowsour.2012.06.097

microscope – TXM located at the beam line X8C, National Synchrotron Light Source (NSLS) – with automated markerless tomography capability [10]. A detailed study of the cathode will be reported elsewhere. The present results show substantial improvements compared to prior TXM fuel cell studies. First, the 40 μm field of view enabled image collection with a total volume of ~25,000 μm^3 to allow a central volume of ~3600 μm^3 for analysis, which is 7–200 times larger than in prior reports (14–512 μm^3 analyzed volume). This provides significantly improved statistics in the resulting morphological data. Second, 1441 projections were collected over a 180° range for a single tomography, considerably improving the 3D spatial resolution; the angular step size of 0.125° was significantly smaller than the typically-used values of 0.5–1° [7]. Third, high image quality combined with dual measurements made above and below the Ni absorption edge allowed for accurate image segmentation via simple thresholding. The Ni–YSZ anode in question was from a high quality anode-supported cell that yielded state-of-the-art electrochemical performance.

2. Experimental

An SOFC consisting of porous 20 μm Ni–YSZ anode functional layer, 8 μm YSZ electrolyte and porous 15 μm LSM–YSZ cathode was prepared in an anode-supported button cell geometry [3]. The SEM cross-sectional image, in Fig. 1 (a) shows the three-layered structure. Electrochemical Impedance Spectroscopy (EIS) and current–voltage (I/V) measurement were carried out on the SOFC. The cell was first operated at 800 °C in air and humidified hydrogen at a current density of 2.6 A cm^{-2} for 16 h, whereupon the cell voltage stabilized at 500 mV. The EIS testing was then completed at 800 °C with the same fuel and oxidant. A Zahner IM6 electrochemical workstation was utilized to collect impedance spectra from a 100 mHz to 1 MHz frequency range, both at open circuit voltage (OCV) and at 0.5 V, near the maximum power density operating point. Additionally, I/V current characteristics were collected at 10 mV increments from OCV to 0 V.

A cylindrical sample with a diameter of about 35 μm and height of about 80 μm was FIB milled from the as-prepared SOFC sample and then removed using a lift-out technique (Supplemental Figure 1). Two tomography measurements, with X-ray energies above and below the Ni absorption K-edge (8400 eV and 8300 eV), were carried out on the SOFC sample at the volume of interest labeled as a square (red online) in Fig. 1(b) (Supplemental Figure 2), to facilitate the segmentation of the Ni, YSZ and pore phases. A standard Filtered Back projection Reconstruction algorithm was used to reconstruct the 3D images.

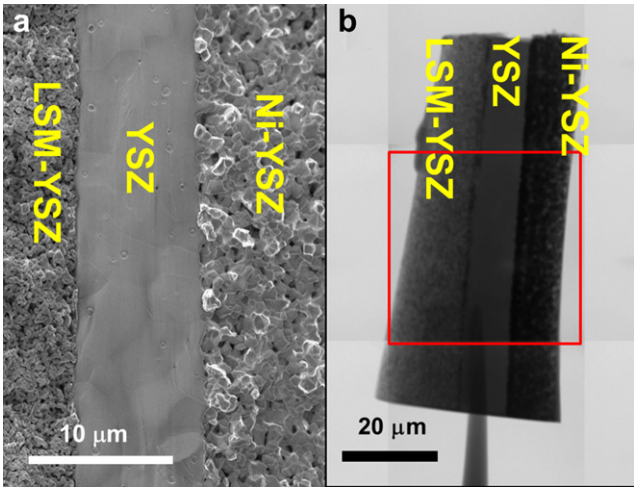

Fig. 1. (a) SEM image of the surface of the SOFC sample and (b) TXM mosaic image projection of the SOFC sample prepared by lift-out in FIB-SEM. The red rectangle highlights the region for tomography measurement. (For interpretation of the references to colour in this figure legend, the reader is referred to the web version of this article.)

3D morphological quantification was then performed to calculate the phase volume fraction, surface and interfacial area density, phase size distribution, directional connectivity. Three phase boundary density was determined and combined with the phase connectivity information to obtain the electrochemically active three phase boundary density, using methods reported previously [1,4,11,12]. The tortuosities of the oxygen ion path in YSZ, and the H_2 gas path in pores, were also determined [13]. Note that the YSZ tortuosity is used to adjust the oxygen ion conductivity within the anode.

3. Results and discussion

The cell voltage and power density versus current density, plotted in Fig. 2a, shows a peak power density at 800 °C under standard conditions (air versus humidified hydrogen) of 1.2 W cm^{-2}. [1] Based on the impedance spectroscopy data shown in Fig. 2b, the cell ohmic resistance is similar at open circuit (0.052 Ω cm^2) and at 0.5 V (0.054 Ω cm^2), values as expected for a 8 μm thick YSZ electrolyte. The cell polarization resistance decreased from 0.30 Ω cm^2 at open circuit to 0.5 V at 0.21 Ω cm^2. This, together with a slight positive curvature of the I/V data in Fig. 2(a), indicates activated electrode processes, although there is a hint of concentration polarization at the highest current density. These results are similar to some of the best anode-supported SOFCs reported in the literature [1], such that the microstructural data presented below is likely representative of such cells.

Anode polarization resistance was estimated by splitting the entire impedance response by a fraction that was measured for very similarly processed full cells. Barfod et al. demonstrated that the Ni–YSZ anode and LSM–YSZ cathode were responsible for 33% and 67% of the non-ohmic response at 700 °C, respectively [14]. Applying their results, our anode resistance was estimated to be between 0.07 and 0.10 Ω cm^2 depending on the bias.

A visual comparison between the reconstructed slices and the segmented slices is shown in Fig. 3. A volume rendering of the reconstruction is shown in Fig. 4(a) with a detailed view of one of the three cropped, segmented volumes of the Ni–YSZ anode shown in Fig. 4(b). Table 1 is the result of the quantitative 3D morphology analysis. The range of morphological parameters are in agreement with the values from studies using FIB-SEM serial sectioning with similar sample preparation [3,4]. The standard error is reported here and demonstrates that large reconstruction volumes, as used in this report, are required to achieve TPB density measurements within 5% error.

Supplementary video related to this article can be found at http://dx.doi.org/10.1016/j.jpowsour.2012.06.097.

The Ni and YSZ phases show little variation in volume fraction, and the average value is consistent with the starting NiO:YSZ ratio, 65:35 wt%. Tortuosity values in Table 1 are averages of the values determined in each of three orthogonal directions; the directional values given in Supplemental Table 2 indicate that the anodes are structurally isotropic, with no preferred transport directions. The intra-connectivity of each phase was evaluated in the relevant direction – pores towards the fuel flow, Ni towards the current collector, and YSZ towards the electrolyte. Fully connected paths to and from a given TPB are required for it to be electrochemically active. The present results show that the volume fractions connected were >99% for all three phases, as expected for a highly

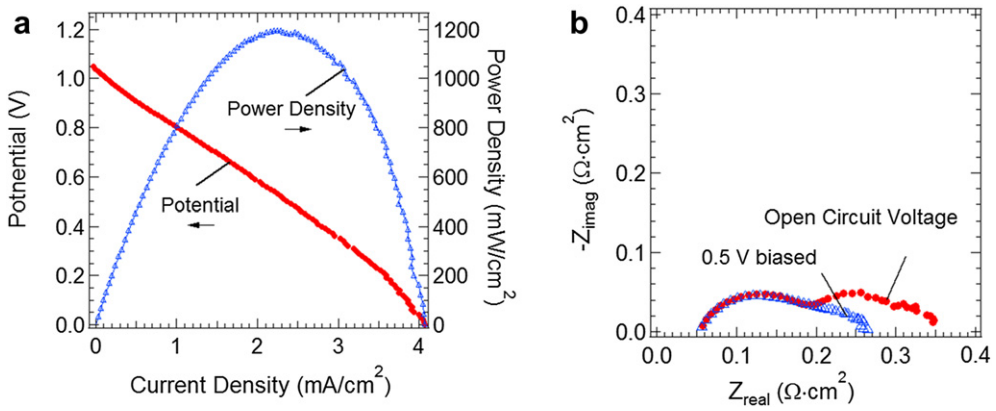

Fig. 2. The electrochemical analysis of the sample 800 °C, humidified hydrogen. (a) *I–V* curve and the power density, (b) the EIS at OCV and the EIS with 500 mV bias.

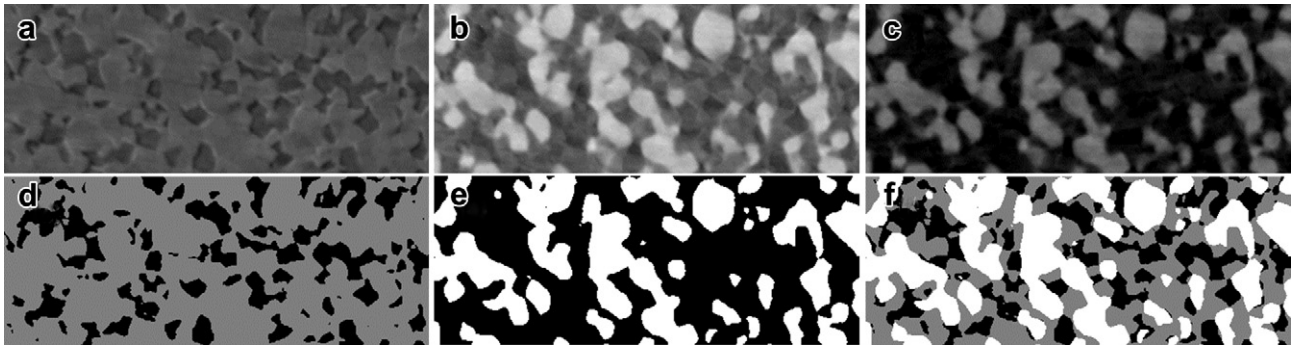

Fig. 3. Reconstructed slices (a) below and (b) above Ni absorption edge. (c) The result of subtracting below edge image from the above edge image, (d) segmented image of (a) to separate the solid phase (Ni + YSZ, gray) from the pore phase (black), (e) segmented image of (c) to isolate the Ni (white) and (f) the final result of segmentation showing Ni (white), YSZ (gray) and pore (black).

optimized high-performance anode. The connected fractions of all three phases are detail in Supplemental Table 1. Finally, Table 1 also gives the total measured TPB density along with the true active TPB density. The latter quantity is obtained from the active, inactive and unknown TPB fractions (Supplemental Table 1), by assessing the fraction of unknown TPBs (those that appear isolated but are at the edge of the measured volume) that are truly active [3,11]. The phase size distribution method was used to show the distribution of the phase size of each individual phase (Supplemental Figure 5). Average size from PSD is calculated from the distribution by averaging the phase size weighted by the volume fraction, which gives the result of: Ni 806 nm, YSZ 507 nm and pore 468 nm.

In order to demonstrate the utility of the measured microstructural data, a porous composite electrode model [15] informed by the averaged microstructural data is used to predict anode polarization resistance. The model simplifies the composite structure as a uniform array of ionic conductor (YSZ) columns decorated with a uniform array of Ni particles. The details of the calculation can be found in Supplementary information 3. Note that no fitting parameters were used in the model. The predicted anode

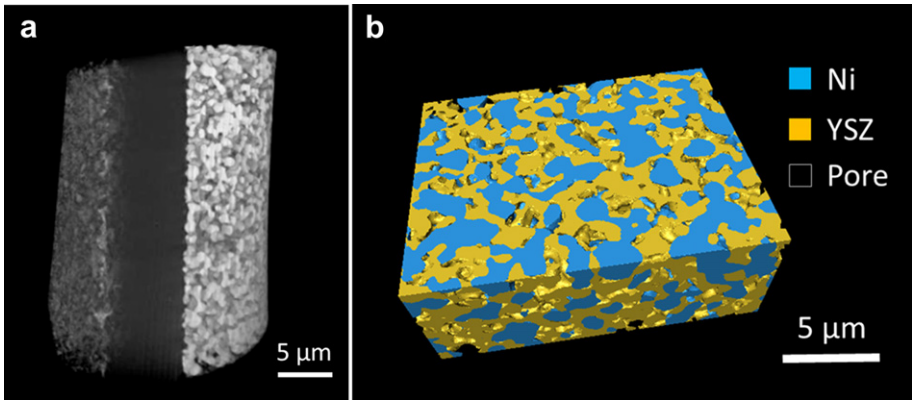

Fig. 4. (a) 3D reconstruction of the SOFC sample from the TXM nano-tomography (video can be viewed online). (b) The 3D morphology of a cropped region from the anode which consists of Ni–YSZ-pore.

Table 1
Quantitative morphological analysis result. Notice that surface area density is defined as phase surface area per total sample unit volume, while the specific area (S_A) is defined as the phase surface area per phase unit volume.

Morphological parameters	Average value	Standard deviation	Error (%)
Individual phase properties			
Volume fraction (%)			
Ni	36.89	0.44	1.21
YSZ	40.09	0.47	1.17
Pore	23.02	0.42	1.83
Surface area density ($\mu m^2\ \mu m^{-3}$)			
Ni	1.52	0.02	1.14
YSZ	2.41	0.01	0.48
Pore	1.74	0.05	2.65
True directional connectivity (%)			
Ni – percolation	99.72	0.08	0.08
YSZ – percolation	99.98	0.01	0.01
Pore – percolation	99.51	0.09	0.09
Average tortuosity ($\mu m\ \mu m^{-1}$)			
YSZ (ion carrier)	1.26	0.01	0.46
Pore (gas path)	1.60	0.01	0.72
Three-phase properties: *triple phase boundary* (*TPB*)			
True active TPB density ($\mu m\ \mu m^{-3}$)	2.89	0.15	5.19
True inactive TPB density ($\mu m\ \mu m^{-3}$)	0.17	0.02	12.57
Active TPB ratio (%)	94.5	0.54	0.57

polarization resistance is 0.062 Ω cm^2 for 800 °C, which is consistent with the measured total polarization resistance at open circuit of 0.3 Ω cm^2 (Fig. 2), considering that the cathode presumably contributed at least half of this resistance.

The electrical conductivity of the composite electrode (σ_c) can also be estimated from the 3D morphological value using the model developed by Mclachlan [16]:

$$\sigma_c = \sigma_{Ni}\left(\frac{V_{Ni} - V_c}{1 - V_c}\right)^t. \quad (1)$$

where σ_{Ni} is the Ni electrical conductivity, V_{Ni} is the Ni volume fraction, V_c is the critical volume percent of Ni and t is the conductivity exponent. As reported in the literature, σ_{Ni} is 25,700 S cm^{-1} (at 800 °C), V_c is 16%, t is 1.6–2.0 [16]. In our sample, V_{Ni} was characterized to be 36.9%, so σ_c can be calculated: 1.59–2.77 × 10^3 S cm^{-1}. The estimated conductivity falls in a range which is consistent with the literature while the conductivity is on the higher end of similar materials [17]. Further modeling [18] and simulation [19–21] work can also be performed based on the 3D morphological parameters reported here.

4. Conclusion

A full field transmission X-ray microscopy with the unique markerless nano-tomography capability developed at NSLS was applied to thoroughly and non-destructively characterize the 3D morphology of a porous Ni–YSZ SOFC anode. 3D resolution and the statistics of the data are considerably improved, which enabled an accurate 3D morphological analysis and quantification of critical parameters. The obtained microstructural data were used in an electrochemical model to predict an anode polarization resistance in good agreement with measured anode resistance. The Mclachlan model is used to estimate the anode electrical conductivity.

Acknowledgments

We thank Dr. Fernando Camino (BNL) and Dr. Can Erdonmez (BNL) for assisting the development of the sample preparation procedure using FIB/SEM. Research carried out in part at the Center for Functional Nanomaterials, Brookhaven National Laboratory, which is supported by the U.S. Department of Energy, Office of Basic Energy Sciences, under Contract No. DE-AC02-98CH10886. We are grateful that Prof. Eric Maire provided us with the ImageJ plug-in for tortuosity calculations. Use of the National Synchrotron Light Source, Brookhaven National Laboratory, was supported by the U.S. Department of Energy, Office of Science, Office of Basic Energy Sciences, under Contract No. DE-AC02-98CH10886.

Appendix A. Supplementary information

Supplementary Material associated with this article can be found, in the online version, at http://dx.doi.org/10.1016/j.jpowsour.2012.06.097.

References

[1] J.R. Wilson, W. Kobsiriphat, R. Mendoza, H.-Y. Chen, J.M. Hiller, D.J. Miller, et al., Nat. Mater. 5 (2006) 541–544.
[2] G.J. Nelson, W.M. Harris, J.J. Lombardo, J.R. Izzo, W.K.S. Chiu, P. Tanasini, et al., Electrochem. Commun. 13 (2011) 586–589.
[3] J.R. Wilson, J.S. Cronin, S.A. Barnett, Scripta Mater. 65 (2011) 67–72.
[4] J.S. Cronin, J.R. Wilson, S.A. Barnett, J. Power Sources 196 (2011) 2640–2643.
[5] H. Iwai, N. Shikazono, T. Matsui, H. Teshima, M. Kishimoto, R. Kishida, et al., J. Power Sources 195 (2009) 955–961.
[6] L. Holzer, B. Munch, B. Iwanschitz, M. Cantoni, T. Hocker, T. Graule, J. Power Sources 196 (2011) 7076–7089.
[7] K.N. Grew, Y.S. Chu, J. Yi, A.A. Peracchio, J.R. Izzo, Y. Hwu, et al., J. Electrochem. Soc. 157 (2010) B783–B792.
[8] P.R. Shearing, J. Gelb, J. Yi, W.K. Lee, M. Drakopolous, N.P. Brandon, Electrochem. Commun. 12 (2010) 1021–1024.
[9] P.R. Shearing, R.S. Bradley, J. Gelb, S.N. Lee, A. Atkinson, P.J. Withers, et al., Electrochem. Solid State Lett. 14 (2011) B117–B120.
[10] J. Wang, Y.-c.K. Chen, Q. Yuan, A. Tkachuk, C. Erdonmez, B. Hornberger, et al., Appl. Phys. Lett. 100 (2012) 143107-1–143107-4.
[11] J.R. Wilson, J.S. Cronin, A.T. Duong, S. Rukes, H.-Y. Chen, K. Thornton, et al., J. Power Sources 195 (2010) 1829–1840.
[12] J.S. Cronin, K. Muangnapoh, Z. Patterson, K. Yakal-Kremski, V.P. Dravid, S.A. Barnett, J. Electrochem. Soc. (2012) (accepted).
[13] E. Maire, O. Caty, A. King, J. Adrien, Iutam Symposium on Mechanical Properties of Cellular Materials, vol. 12 (2009) 35–42.
[14] R. Barfod, M. Mogensen, T. Klemenso, A. Hagen, Y.L. Liu, P.V. Hendriksen, J. Electrochem. Soc. 154 (2007) B371–B378.
[15] C.W. Tanner, K.Z. Fung, A.V. Virkar, J. Electrochem. Soc. 144 (1997) 21–30.
[16] Y. Guan, W.J. Li, Y.H. Gong, G. Liu, X.B. Zhang, J. Chen, et al., J. Power Sources 196 (2011) 1915–1919.
[17] D. Simwonis, F. Tietz, D. Stover, Solid State Ionics 132 (2000) 241–251.
[18] X.H. Deng, A. Petric, J. Power Sources 140 (2005) 297–303.
[19] H.Y. Chen, H.C. Yu, J.S. Cronin, J.R. Wilson, S.A. Barnett, K. Thornton, J. Power Sources 196 (2011) 1333–1337.
[20] A.S. Joshi, K.N. Grew, A.A. Peracchio, W.K.S. Chiu, J. Power Sources 164 (2007) 631–638.
[21] D. Kanno, N. Shikazono, N. Takagi, K. Matsuzaki, N. Kasagi, Electrochim. Acta 56 (2011) 4015–4021.